Induced Microearthquake Patterns in Hydrocarbon and Geothermal Reservoirs

W. Scott Phillips

James T. Rutledge

Leigh S. House

Michael C. Fehler

Seismic Research Center

Los Alamos National Laboratory

Submitted to PAGEOPH

March, 2000

LAUR 00-1328

Abstract

The injection or production of fluids can induce microseismic events in hydrocarbon and geothermal reservoirs. By deploying sensors downhole, data sets have been collected that consist of a few hundred to well over 10,000 induced events. Automatic or routinely determined event locations often form diffuse, cloud-like patterns; however, after carefully redetermining arrival times, we find that most induced events cluster in well defined geometrical patterns. At three sedimentary sites, location patterns are dominated by thin horizontal strands. We believe this reflects fracture containment between stratigraphic layers of differing mechanical properties. At a massive carbonate and two crystalline sites, combinations of linear and planar features outline networks of intersecting fractures and allow us to infer positions of aseismic fractures through their influence on the location patterns. In addition, the seismicity patterns often evolve systematically with time. At sedimentary sites, migration of seismicity toward the injection point has been observed and may result from slip-induced stress along fractures that initially have little resolved shear. In such cases, triggering events are critical to generate high levels of seismic activity. At one crystalline site, the early occurrence of linear features that traverse planes of activity indicate permeable zones and possible flow paths within fractures. We hope the continued development of microseismic techniques and refinement of conceptual models will further increase our understanding of fluid behavior and lead to improved resource management in fractured reservoirs.

Running Head: Microearthquake Patterns in Reservoirs

Key Words: induced microseismicity, geothermal, oil and gas, fluid flow, location

Introduction

Microseismic monitoring has been carried out during the hydraulic stimulation of experimental hot-dry-rock geothermal reservoirs since the mid-1970's (Pearson, 1981; Albright and Pearson, 1982). Mapping the cloud of microseismicity proved valuable in estimating the rough extent and orientation of a stimulation. For example, a 1983 stimulation (21,000 m^3) at Fenton Hill, New Mexico yielded over 11,000 locatable seismic events. The mapped event cloud formed a 0.3 km^3 tabular volume surrounding the injection point; however, the cloud did not extend to a nearby well, located 200 m distant (House, 1987). Neither was an intended fluid connection observed in that well. Later, a sidetracking operation was performed to drill into the seismic cloud, where a flow connection was established between the wells, allowing circulation of the man-made geothermal reservoir.

Although microseismic clouds have played a key role in the development of hot-dry-rock geothermal reservoirs, these results produced little information concerning the intricacies of the fluid-flow network. Recently, high-precision relative location techniques have been successfully applied to geothermally induced events, offering the ability to observe patterns at unprecedented levels of spatial detail (Phillips et al., 1997; Tezuka and Niitsuma, 1997; Li et al., 1998; Gaucher et al., 1998; Lees, 1998). To make practical use of these results, we must ascertain the detailed relationships between seismicity, fracture geometry, stress and fluid flow. We generally rely on simple interpretive models, such as that in which increased pore pressure reduces normal stress and causes slip (Pearson, 1981). Thus, the presence of seismicity at a given location is taken to indicate a pressure connection, but not necessarily a high-permeability connection, between that location and the injection well. Furthermore, this model predicts little shear-slip seismicity along fractures that open in tensile mode, potentially the most conductive flow paths. As experience is

gained in interpreting high-precision location patterns, we hope to better use the patterns to infer locations of high-flow paths, even if those paths are seismically inactive.

The successful application of microseismic observation techniques in hot-dry-rock geothermal reservoirs is partially attributed to the simple and efficient propagation paths through the host crystalline rock. Microseismic techniques might be equally useful in sedimentary, hydrocarbon reservoirs if sufficient numbers of events can be observed. Of course, the more complex and less efficient propagation through sedimentary rock should degrade waveforms; however, successful experiments have been run for years (Dobecki, 1983; Sarda et al., 1988; Fix et al., 1989; Vinegar et al., 1991; Warpinski et al., 1996; Zhu et al., 1996; Maxwell et al., 1998; Dyer et al., 1999) and a number of recent experiments have collected data sets of sizes similar to geothermal data sets, given the volumes of injected fluid (Figure 1). These encouraging results should lend impetus to studies relating high-precision seismicity patterns, fracture systems and fluid flow in hydrocarbon reservoirs.

In this paper, we summarize location results from six case studies: four in sedimentary and two in crystalline environments. In most cases, event locations that initially formed cloud-like patterns collapse into simple geometrical shapes, generally point clusters, line segments, planar patches or combinations thereof. We speculate on the mechanisms that might produce the observed patterns, with the goal of better understanding fluid flow in fracture systems.

Microseismic Data and Location Methods

Because of their small size, induced microearthquakes must be monitored using borehole instruments located close by. The larger induced events approach a magnitude of +1, while most events fall in the magnitude -4 to -2 range, varying somewhat with

experiment. Large shear waves and the presence of both compressional and dilatational first arrivals indicate that most induced events have dominantly shear-slip mechanisms. Tensile mechanisms have been observed during some stimulations; however these events produce relatively little seismic energy and display a distinctive spectral peaking that reflects modes of the fluid filled crack (Bame and Fehler, 1986; Ferrazzini et al., 1990). From spectral studies, Fenton Hill shear-slip events have moments 10^{13} to 10^{18} dyne-cm, source radii 1-100 m and Brune stress drops 0.1 to 20 bars (Fehler and Phillips, 1991). Furthermore, Fehler and Phillips (1991) found that small events dominated the energy release at Fenton Hill (high Gutenberg-Richter b-value). This behavior is similar to what is often observed in earthquake swarms and volcanic sequences and is consistent with pronounced small-scale heterogeneity in permeability and pore pressure along fracture surfaces (Sykes, 1970). Thus, induced failure often occurs as a sequence of many small events rather than a few large events, allowing the use of event location patterns to delineate the geometry of slipping joints or fractures.

The requirement for downhole recording imposes a severe restriction on monitoring. Success has been achieved with only one geophone; however, three or more geophones in two or more wells are required to perform high-precision location (two stations in different wells can be sufficient if reflected arrivals are observed, as a later example will show). The sparse monitoring networks make it necessary to use shear waves, and occasionally, reflected phases and particle motion (hodogram) data, to locate events. In addition, coupling effects are difficult to control in wellbores and we often see spectral peaks in the data (monochromatic waveforms), perhaps caused by a poor bond between the well casing and the formation. In recent years, some microseismic experiments have been run using multi-level geophone strings that are cemented into wells expressly drilled for or sacrificed to monitoring (e.g. Keck and Withers, 1994). This type of deployment can give excellent

depth constraint on locations and minimizes coupling related effects, but is much more expensive than temporary deployments in existing wells.

Although the downhole recording environment has drawbacks, avoiding the scattering and low attenuation of near surface materials can yield simple and easily interpreted waveforms. Furthermore, we generally observe that waveforms from nearby events are very similar to one another, likely the result of common paths and source orientations (Moriya et al., 1994; Roff et al., 1996). Relative arrival times of similar waveforms can be precisely determined, which, in turn, allows high precision relative locations to be calculated. Figure 2 shows vertical component seismograms from two areas of the Fenton Hill reservoir. Consistent P- and S-wave arrival times can be chosen by marking the same point in the waveform for all events. Conversely, timing the events in order of occurrence as is normally done during routine processing, would result in inconsistant picks because the similarities between waveforms would not be noticed. This is especially apparent for the S waves from the second group shown in Figure 2.

We determine arrival times manually using a procedure that approximates the precision of automatic cross-correlation schemes through choosing waveform peaks rather than first breaks. In tests on Fenton Hill data, applying a cross-correlation method (after VanDecar and Crosson, 1990) produced virtually no change in the relative location pattern compared to results determined originally by visual cross-correlation. When picking times manually, looking at larger events first helps to identify waveform shapes that are more difficult to find in poorer signal-to-noise traces. We also experiment with filters to enhance the visual similarity of waveforms. With events that display poor waveform correlation, the peak following the first break is chosen irrespective of polarity. Poor correlation is common and can most often be attributed to near nodal takeoff angles. Automatic, high-precision timing methods are being investigated with downhole data sets (starting with initial arrivals

rather than high-precision arrivals as for the test mentioned above); however, to date, direct comparisons show the automatic results provide less interpretable detail than can be obtained manually. Possible reasons and implications of this will be discussed later.

Calibration is a critical component of microseismic location. This involves determining velocity structures, station corrections and geophone orientations if particle motion information is to be used in location. Calibration is less important for relative location studies because path effects can be assumed to be similar. However, the absolute locations of the resulting event patterns are likely to be more uncertain than are their relative locations.

To calculate relative locations, we use the master-event technique (Evernden, 1969). This only requires a generic event location code. An event with the largest number of high-quality arrivals is chosen as the master. The hypocenter of this event is fixed at some initial location and station corrections are set equal to the arrival-time residuals for each station and phase type. These station corrections are then applied to the remaining events to obtain locations relative to the master event. Next, sizes, shapes and orientations of the location error ellipsoids are examined to eliminate systematic error as the source of any patterns that may be observed. We approximate errors by assuming the locations are perfectly calibrated absolute locations. First, relative data errors for each station and phase type are estimated based on the frequency content and degree of similarity of the filtered waveforms used to determine arrival times. After computing locations using weights based on the relative errors, a constant multiplier is applied to produce absolute arrival-time errors that best match rms residuals for the full data set. We have assumed that the frequency content of the seismograms more directly controls relative arrival error than do signal-to-noise effects. This is a valid assumption because poor signal-to-noise waveforms that display little similarity with the rest of the data are eliminated from the study.

Results

We present high-precision locations from six experiment sites. Four are sedimentary, the other two are crystalline environments. In five cases, microseismic events were induced by fluid injection; in one case (Clinton County, Kentucky), events were induced by oil production. In three of the six cases, precise relative locations are necessary to see detailed patterns in the microseismicity.

Austin Chalk, Giddings Field, Texas

The Austin chalk is a fractured limestone with a matrix porosity of 10% and matrix permeability of 0.01 to 0.1 millidarcys. Fractures result from the bending of the brittle limestone over a deeper and older Jurassic shelf margin, which trends northeast-southwest, roughly parallel to the Gulf coast of Texas. These fractures enable the Austin chalk to produce oil at relatively high rates (up to 160 m^3 per day) and reach single well maximum cumulative production approaching 80,000 m^3 of oil. Hydraulic stimulation is used to complete new wells and to enhance production from older wells. During stimulation, the water forced into untapped areas of the chalk is thought to replace, and thus mobilize hydrocarbons residing in small cracks through imbibition.

To study the stimulated fracture systems, we monitored Austin chalk microseismicity during two 4000 m^3 stimulations at depths greater than 2000 m in the Giddings field (Phillips et al., 1998). We deployed a single three-component geophone at one site and two geophones in separate wells at a second site. Over 480 and 770 microearthquakes were collected during the two stimulations. Many seismograms included an S-wave reflection off a high contrast interface below the Austin chalk.

At the two-geophone Giddings site, arrival times from P, S and reflected phases allowed events to be located in three dimensions without having to rely on particle motion (hodogram) constraints. Locations of 90 high-quality events aligned with the expected fracture trend and extended over 800 m from the injection point (Figure 3). Event depths were constrained to a narrow range along the base of the Austin chalk. In this area, reservoir engineers rely on a thin, ductile layer of volcanic ash embedded within the Austin chalk to contain the stimulation to the deeper, producing portion of the Austin chalk. The Eagleford shale limits the stimulation at the base of the Austin chalk. The tight depth distribution of microearthquake locations demonstrates that containment was effective at this site.

To increase the number of locatable events, we fixed event depths to injection depths and obtained densely populated seismic zones that aligned with the expected fracture trend at both sites. However, the seismic zone at the first site was five times wider (horizontally) than the zone at the second site shown in Figure 3. There was a large increase in the oil production rate from the first site immediately following stimulation, but little increase from the second (Phillips et al., 1998). This suggests that the width of the microseismic pattern reflects the degree to which ancillary fractures are accessed, and thus indicates the lateral extent and effectiveness of the stimulation.

Frio Formation, Texas

In October 1993, an injection experiment was performed in Jasper County, near Beaumont, Texas (Keck and Withers, 1994). The purpose of this experiment was to investigate the safe use of hydraulic fracturing for solid waste disposal. To accomplish this, an injection well and two monitoring wells were drilled to depths of 1460 m. Fluids (8000 m^3) and solids were injected into the highly permeable and unconsolidated Lower Frio

sandstone over a depth interval of 1349 to 1407 m. The Lower Frio was bounded above and below by relatively impermeable shales.

Induced microearthquakes were continuously monitored to determine the lateral extent and the height of the fracture system that was produced (Withers and Rieven, 1996; Rieven, 1999). Each monitor well contained 25 three-component geophone packages at 9 m (30 ft) intervals that were cemented in. Nearly 2900 seismic events were recorded during the entire experiment. Most were too small to be located reliably. A total of 54 well-recorded microearthquakes were chosen for further study, based on numbers of P- and S-wave arrivals (House et al., 1996; House and Flores, 2000).

Epicenters of the 54 high-quality events, located using P and S arrival times, extend about 200 m southwest from the injection well (Figure 4). The near-injection seismicity scatters around the injection well, while a distant cluster falls along a narrow, horizontal trend, aligned toward the injection borehole. The tight hypocentral distribution of the distant cluster is surprising, because one would expect that the unconsolidated nature of the Frio Formation would not support the development of such a well-defined zone of deformation (House et al., 1996). Withers and Rieven (1996) report a temporal migration towards the injection well within this group of events, and similar behavior for a second cluster recorded during a later injection.

Cotton Valley, Texas

In May, 1997, a consortium of operators and service companies conducted an extensive hydraulic fracture imaging demonstration in the Cotton Valley tight gas sands of East Texas (Walker, 1997). Well completions and re-completions in this type of reservoir

account for many of the hydraulic fracture operations conducted in the United States and, therefore, constitute an important potential application of microseismic techniques.

At this site, two 48-level, 3-component geophone arrays were cemented behind the casing of two offset monitor wells. We analyzed microseismicity recorded during the second of three injection stages, a 1100 m^3 injection at depths of 2757 m to 2838 m. Nearly 1200 events were detected and 290 were initially located (Rutledge et al., 1998a). The locations show a diffuse, tabular feature striking N70°E and dipping 45° SE.

A tight cluster of 161 events located 120 m east of the treatment well generated similar P and S waveforms. For this cluster, we manually determined relative arrivals to sub-sample precision using data from 6 stations representative of both monitor well arrays. After applying the master-event location technique to the P- and S-wave data, locations collapse into a thin horizontal strand, 40 m long and less than 3 m thick (Figure 5). The events separate into two main groups (blue and red, Figure 5), distinguished by a change in S waveform character at one station. The change could result from the variation in takeoff angles from one end of the feature to the other, a near-source path effect, or a change in source mechanism. A third group (green) generated waveforms dissimilar to the first two. The linear feature is especially well defined along its western half and breaks into small subclusters in the eastern half. A slight bend can be seen toward the eastern end. Location error ellipsoids are oriented along the trend, as expected for the station geometry, but are of magnitude less than 2 m.

Fracture growth patterns are revealed by the remarkable temporal behavior of the relocated events (Figure 6). The seismicity begins at the eastern end, near the bend (Figure 5), then migrates westward toward the injection well. In the eastern half of the cluster we observe three subclusters that rupture repeatedly. Within each sub-cluster, similar sized

events occur and also appear to migrate westward. The subclusters may represent discrete, isolated fractures separated by a few meters, with event sizes within each sub-cluster being limited by fracture dimension. These patterns would be obscured if location error were any more than a few meters, which further supports the resolving power of the relative mapping method. A third set of events, distinguished by waveform types that were less similar to the two main groups, occurs when the injection well is shut in.

Clinton County, Kentucky

In Clinton County, Kentucky, oil is produced from low porosity carbonate rocks of Ordovician age, at depths from 230 to 730 m. A preponderance of isolated, high volume wells suggests the existence of isolated zones of fracture storage and high permeability. Initial production rates as high as 64 m^3 per hour and cumulative production of 16,000 m^3 from a single well have been reported (Hamilton-Smith et al., 1990). However, fracture orientations are generally unknown and are often assumed to be vertical. We deployed geophones near high volume producing wells at a number of Clinton Co. sites with the goal of delineating the reservoir fracture systems (Rutledge et al., 1998b).

Three geophones were deployed in two existing wells at depths between 240 and 430 m at the Tallent site in Clinton Co. and monitoring started six weeks after a nearby well began production. Over 3200 events were recorded during a period of 28 weeks. The event rate was clearly associated with the production rate, but with a lag of two to three weeks (Rutledge et al., 1998b). Events may have been triggered by tiny increases in horizontal compressive stress associated with the depletion of an adjacent fracture, or by small pore pressure changes associated with the replacement of oil by brine (Rutledge et al., 1998b).

The Tallent site was calibrated using shot and well log data and a hypocenter-velocity inversion applied to a high-quality subset of events. Following this, events were located using absolute location techniques; over 1200 of the best quality locations are shown in Figure 7. Results show three fracture planes striking N65°E to N82°E and dipping 15° to 20° to the NW or to the SE that surround, but do not intersect, the producing interval. Relatively few events populate the deepest fracture (200 events total; 80 high-quality locations are shown in green, Figure 7), but unique, S-nodal (large P, small S) waveforms observed at one geophone distinguish these events from those of the main group (shown in red). The deep event group forms an elongate planar pattern that intersects the main fracture along its northern, well-defined edge.

The seismically active fractures can be extrapolated to old production intervals in wells from which 725 m^3 of oil had been extracted in the nine months preceding monitoring. Two wells were later drilled into the main mapped fracture and produced brine. Thus, the microearthquake locations defined fractures that had contained oil, but were drained and subsequently recovered to hydrostatic pressure via brine invasion. If knowledge of the fracture orientation can be extrapolated to other sites in this region, these results should aid field development by improving drilling strategies (horizontal drilling will help little, for example), placement of offset wells and abandonment or pressure maintenance operations to avoid premature contamination of producing wells by brines.

Fenton Hill, New Mexico

In December 1983, a massive hydraulic fracturing (MHF) experiment was carried out at the hot-dry-rock geothermal site at Fenton Hill, New Mexico. Over 21,000 m^3 of water were injected in 61 hours. The injection point was 3460 m deep in predominantly granitic, Precambrian basement under the southwest flank of the Jemez caldera. The

purpose of the hydraulic fracturing was to create a reservoir through which fluids could be circulated to extract geothermal heat (Dreesen and Nicholson, 1985; Franke and Nunz, 1985).

The MHF experiment was instrumented with both shallow and deep borehole sensors to monitor accompanying seismic activity (House, 1987). Two vertical-component sensors were sited near the top of the basement at depths greater than 500 m and two pressure- and temperature-hardened, triaxial sensors were sited within the basement at depths of 2855 m and 3300 m. Over 11,000 locatable microearthquakes were recorded. They filled a tabular volume, 1 km by 1 km by 300 m in size, striking N10°W and dipping 65° to the east.

Precise relative location techniques were applied to five clusters within the microseismic cloud (Phillips et al., 1997). In all cases, initially scattered hypocenter patterns tightened dramatically after repicking and relocation. The example shown in Figure 8 is small in extent, but otherwise typical of the five clusters. Events fall onto an isolated planar patch about 50 m across. In the face-on view (bottom right in Figure 8), sharp, straight edges bound the planar patch, roughly forming a parallelogram. This bounding edge pattern was seen in four of the five cluster studied; in the fifth cluster, events fell onto a single, isolated linear segment. The edges of the planar clusters likely result from truncation of the slipping surface by aseismic joints. Thus, the seismicity allows some constraint on position and orientation of the aseismic joints, which may form part of the fluid-flow network. The isolated linear segment is thought to occur along the intersection of two otherwise aseismic joints. This conclusion had been drawn earlier by Roff et al. (1996) after examining many linear and planar features in the original, full data set.

Soultz-sous-Forêts, France

The Soultz-sous-Forêts geothermal site is located in the Alsace region of France, along the western edge of the Rhine Graben at a point where especially high subsurface temperature gradients can be found. At Soultz, the reservoir region lies in granitic rock at depths of 2 to 4 km. Temperatures reach 168° at a depth of 3.8 km. In September 1993, 44,000 m^3 of water was injected at a depth of 2850 m in the first stage of reservoir creation (Jung et al., 1996).

During injection, seismic activity was recorded by three, four-component borehole sensors and one borehole hydrophone deployed at depths between 1.3 and 2.1 km. Over 16,000 events were recorded. The seismic cloud is tabular in form, with dimensions of about 1.5 by 1.2 by 0.5 km, strikes NNW and dips nearly vertically (Jones et al., 1995). The overall shape is similar to that observed for the MHF injection at Fenton Hill.

A cluster analysis based on spatial locations identified numerous concentrations of microearthquake activity throughout the September 1993 cloud of seismicity. Two of these clusters were chosen for a precise relative location study (Phillips, 2000). Relative P- and S-wave arrival times were determined manually, imitating cross-correlation picking when possible, and choosing first break peaks for data that were inconsistent or nodal. For the deeper if the two clusters, events were grouped based on S waveform shapes at one station, and these groups became spatially distinct after location.

Following relative event relocation, the clusters collapsed into well-defined patterns made up of planar features (Figure 9). Both clusters consist of two planar patches that intersect and terminate against one another, as seen in views along the trends of the planar intersections (Figure 9, top). Linear segments within the seismicity become apparent in the broadside views (Figure 9, bottom), possibly indicating cross-cutting fractures. The slip

inferred from focal mechanisms causes a mass deficit on the inside corner of the planar intersections and acts to decrease normal stress, perhaps resulting in further slip. This effect is most obvious for the deep cluster and may be the mechanism responsible for the high levels of activity.

Both clusters display remarkable temporal behavior. Events are color coded by the order in which they occur in the face-on views (Figure 9, bottom). In the shallow cluster, most of the earliest events fall along two linear segments. Activity began along these segments and spread into the planar patches as the pressurization continued. In the deep cluster, activity began on plane 4 along linear segments and tailed off with a shift of activity to plane 3. Activity continued along linear segments and spread in between with time. The early activity along linear segments indicates their association with permeable zones within the fracture. The confinement of flow to narrow channels had been predicted by modeling studies (Kohl et al., 1997). If one may extrapolate these results to the entire reservoir, linear segments could indicate important components of the fluid-flow network at Soultz and mapping their distribution should lead to important advances in understanding reservoir behavior.

Discussion

In a massive, competent limestone and in crystalline environments we observe seismicity that organizes into combinations of linear and planar features. At Fenton Hill, straight, nearly parallel edges bound planar patches of activity (Figure 8) and have been interpreted as representing aseismic joint sets that truncate the seismically active joints. The planar patches are isolated from other seismicity, but, in one cluster, a unique family of events falls along one edge (Phillips et al., 1997), possibly representing slip on the truncating joint. One or more of the aseismic, truncating joints could have acted as pressure

conduits to the otherwise isolated patches. Thus, these aseismic joints could be part of the fluid network and their positions and orientations can be partially constrained by patterns in the seismically active joints. Results from Soultz and Clinton Co., Kentucky, support the truncation model, although, at these sites, the truncating features are seismically active. In both cases, planar zones of seismicity truncate each other and form "V-shaped" patterns when viewed along the intersection trend. At Soultz, we observe additional linear features within the seismically active fractures. These could be traces of intersecting, aseismic joints, but could also mark changes in rock composition, such as small dikes. Either way, the linear segments represent permeable channels within fractures because they are observed to develop early in the injection. Thus, precise event locations allow us to do more than simply ascertain the position, orientation and extent of active fractures, they also allow us to constrain positions of aseismic fractures that may be permeable, as well as make inferences as to fluid-flow paths within fractures.

In clastic sedimentary environments, we observe a strong tendency for induced microseismicity to organize into thin horizontal strands of activity. This behavior is especially surprising in the Lower Frio, given the unconsolidated nature of these sediments, as noted by House and Flores (2000). From studies in crystalline environments, linear features are thought to occur along intersections between otherwise aseismic fractures; however, this mechanism gives rise to a multitude of possible linear orientations. The near horizontal orientations found consistently at the clastic sedimentary sites leads us to suspect that stratigraphy, instead, controls the behavior. Stratigraphic changes can limit fracture growth through an increase in ductility or an increase or decrease in mechanical strength and supported stress at a layer boundary. The observed confinement of microseismic events between the tuff and shale layers within and below the Austin chalk, respectively, support this interpretation. Similar effects have been demonstrated in fracture mine back experiments (Warpinski and Teufel, 1987). We propose that this also controls the linear

patterns observed in the Cotton Valley and lower Frio studies. We look forward to refining these ideas as additional field information, including comparison with well log stratigraphy, fracture and flow data, is included in these studies.

Strong spatio-temporal relationships have also been observed at sedimentary sites. The observed patterns lend credibility to the estimated location accuracy and may yield important insight into microseismic generation. One of the more intriguing temporal behaviors is the systematic migration of events towards the injection well at Cotton Valley. Withers and Rieven (1996) also report migration of seismicity towards the injection well within two, separate clusters of activity in the Lower Frio. We might expect migration, if it were due to fracture extension, to evolve away from the active well with time. Such behavior is observed, but only during early stages of injection in the Lower Frio (Rieven, 1999). A possible interpretation of the reverse migration is that the inflating fracture is oriented normal to the minimum principal stress and supports little resolved shear, in which case initial slip requires a particular mechanical condition that occurs infrequently along its length. Alternatively, Withers and Rieven (1996) observe that events increase in size with distance from the injection point during pressurization of the Lower Frio and propose that this results from an increasing accumulation of energy at the fracture tip with time. In either case, once slip has initiated at a distant point, local stresses are altered in both directions along the fracture, increasing the potential for slip. Migration towards the well may occur preferentially because pore pressure is higher in that direction. Thus, because reverse migration is commonly observed, slip-induced stresses can be responsible for significant fractions of the seismicity along inflating fractures oriented perpendicular to the minimum stress.

The effects of seismic slip on the local stress field may also be important at the Soultz site, where we observe concentrations of seismicity where fractures intersect. Focal

mechanisms show that the seismic slip would cause a mass deficit at the inside corners of fracture intersections, which means slip on either fracture would reduce normal stresses on the other fracture and would facilitate additional slip events. This mechanism could also explain the high seismicity in the Cotton Valley cluster, where the initial slip occurs near a slight bend at the eastern end of the linear segment, although further study is needed to confirm this interpretation. Thus, slip-induced stress could cause the systematic migration discussed previously, as well as the clustering patterns we observe. It could ultimately affect the flow network in some cases and should be an important focus for future quantitative work.

Significant progress has been made recently in the development of methods that rely on routinely determined event hypocenters to find details in clouds of seismicity. The three-point method (Fehler et al., 1987) finds planar orientations by examining all combinations of three hypocenters at a time. The orientations of Fenton Hill planes found with this technique are consistent with known stress fields. The collapsing method (Jones and Stewart, 1997) shifts hypocenters toward the center of mass of nearby events and is able to resolve numerous geometrical features that are otherwise obscured by location error. This method has been generalized into a joint hypocenter (JHD) method (Fehler et al., 2000). Another method that identifies clusters of events based on S-to-P amplitude ratios found many small linear and planar clusters that matched orientations obtained by applying the three-point method to a Fenton Hill data set (Roff et al., 1996). Of these methods, collapsing is the easiest to apply. The positions and orientations of planar features obtained using the collapsing method have been shown to agree with those obtained by precise arrival time repicking (Fehler et al., 2000); however, repicking reveals an extra level of complexity, such as the bounding edges and linear features within planes, upon which much of our interpretation is based.

Precise manual repicking of arrival times requires painstaking attention to detail and, depending on the data set, can take considerable time. As many as 1000 events can be reasonably processed in this manner. However, for large data sets, such as the 16,000 events in a single injection at Soultz, manual methods become impractical. Automated methods must be investigated for this reason. Automated, cross correlation repicking methods have been successfully applied to natural earthquake data sets (Dodge et al., 1995; Shearer, 1997; Rubin et al., 1999), but have been less successful with induced data sets. Induced events from the same geometrical feature often produce waveforms that correlate poorly at one or more stations, even though waveforms at other stations might display high levels of similarity. This primarily results from near nodal takeoff angles to those stations (Rutledge et al., 1998b; Phillips, 1999), but perhaps also from near source path variation or varying slip directions along the fracture due to stress heterogeneity. The poorly correlated waveform arrivals are necessary to constrain hypocenters and cannot be discarded, as can be done in natural earthquake studies for which many more stations are generally available. Furthermore, downhole site conditions can yield band-limited seismograms, which causes difficulty in identifying the correct cycle when aligning waveforms (cycle skipping). Manual picking is better able identify consistent nuances in such waveforms that allow their alignment. Because the eye is able to identify these nuances, it should be feasible to modify automatic relative picking methods to do the same. Automatic methods are currently being tested on the Soultz deep cluster data set shown in Figure 9 and are being compared to results from our manual repicking (Aster and Rowe, 2000). This work is showing that relative event locations obtained automatically reproduce the intersecting planes shown in Figure 9, but must be developed further to obtain the finer scale features such as the linear segments that we find important for interpretation. However, the automated methods show much promise and, with further development, should allow large data sets to be precisely located in a timely fashion.

Conclusions

In our experience with induced events in geothermal and hydrocarbon reservoirs, the diffuse seismicity patterns that are seen in routinely processed data sets collapse into distinct geometrical patterns after arrival times are precisely repicked. While the repicking shifts arrival times only a fraction of the dominant period, it can improve location patterns significantly. This can be particularly important when few stations are available, as is common for induced seismicity data sets. The large number of small events (high Gutenberg-Richter b-value) that are generally observed (e.g. Fehler and Phillips, 1991) means that abundant events are available to delineate slip surfaces and boundaries well. We suggest that routinely determined location patterns and subsequent interpretations will be considerably improved by carrying out precise relative locations with any induced data set. Furthermore, interpretations crafted to be consistent with diffuse seismicity should be viewed with this possibility in mind.

We find that horizontal, linear features dominate the seismicity patterns in clastic sedimentary environments common to oil and gas reservoirs. Well-defined temporal migration of the seismicity, most often towards the active well, also is observed at these sites. We believe the linear patterns result from stratigraphic variations that confine the stimulated fractures and the migrating seismicity results from slip-induced stress concentrations that are initiated by triggering events. In some cases, the low resolved shear stress on a fracture oriented orthogonal to the least principal stress may require a triggering event to produce significant amounts of seismicity. Such a triggering event may occur where conditions are locally more favorable for slip, such as at a bend in the fracture.

In crystalline rock and massive, brittle sediments, the location patterns indicate interacting networks of fractures. Not only can active fractures be identified and mapped,

but the positions and orientations of aseismic fractures also can be inferred through the imprints they leave in the seismicity patterns, namely, the straight edges bounding the seismically active planar patches or the linear segments that cut though them. Aseismic fractures could be important components of the fluid-flow network. Linear zones within seismically active fractures are observed to develop early and could mark permeable channels along fracture intersections at the Soultz geothermal site. Therefore, in addition to constraining the geometry of the fracture network, seismicity can also be used to infer zones of higher permeability.

The mapping of large data sets, such as Fenton Hill and Soultz, to the level of precision demonstrated here will rely on the development of automatic methods. Waveform cross-correlation methods have shown much success with natural earthquake data sets. However, induced seismicity data sets present more difficulty because of the small number of stations that are available. This means that all arrivals must be relied upon to constrain event locations, even if nodal takeoff angles produce poorly correlated waveforms or if wellbore site conditions produce band-limited waveforms at particular stations, as is commonly observed. Manually determined arrival times can be used to guide the further development of automatic methods that will more reliably align such waveforms (Aster and Rowe, 2000).

Acknowledgments

We are grateful to Professor Hiroaki Niitsuma and members of the MTC project for their advice and encouragement. We also thank Dave Anderson, Tom Fairbanks, Jim Albright and Bob Hanold for their operational and technical support. This study was partially supported by the DOE Oil Recovery Technology Partnership and the DOE Office of Basic Energy Sciences.

References

Albright, J. N. and Pearson, C.F. (1982), *Acoustic emissions as a tool for hydraulic fracture location: Experience at the Fenton Hill Hot Dry Rock site*, J. Soc. Pet. Eng., *22*, 523-530.

Aster, R.C. and Rowe, C.A. (2000), *Automatic phase pick refinement and similar event association in large seismic datasets*, in: C. Thurber and N. Rabinowitz, eds, Advances in Seismic Event Location, *in press*.

Bame, D. and Fehler, M.C. (1986), *Observations of long-period earthquakes accompanying hydraulic fracturing*, Geoph. Res. Lett., *13*, 149-152.

Dobecki, T. L. (1983), *Hydraulic fracture orientation by use of passive borehole seismics*, paper SPE 12110, presented at the 1983 SPE Annual Technical Conference and Exhibition, San Francisco.

Dodge, D.A., Beroza, G.C. and Ellsworth, W.L. (1995). *Foreshock sequence of the 1992 Landers, California, earthquake and its implications for earthquake nucleation*, J. Geophys. Res. *100*, 9865-9880.

Dreesen, D. S., and Nicholson, R.W. (1985), *Well completion and operations for MHF of Fenton Hill well EE-2*, Trans. Geotherm. Res. Coun., *9, Pt II*, 105-110.

Dyer, B.C., Jones, R.H., Cowles, J.F., Barkved, O. and Folstad, P.G. (1999), *Microseismic survey of a North Sea reservoir*, World Oil, *March*, 74-78.

Evernden, J.F. (1969), *Identification of earthquakes and explosions by use of teleseismic data*, J. Geophys. Res., *74*, 3828-3856.

Fehler, M. C., and Phillips, W.S. (1991), *Simultaneous inversion for Q and source parameters of microearthquakes accompanying hydraulic fracturing in granitic rock*, Bull. Seism. Soc. Am., *81*, 553-575.

Fehler, M. C., House, L.S. and Kaieda, H. (1987), *Determining planes along which*

earthquakes occur: method and application to earthquakes accompanying hydraulic fracturing, J. Geophys. Res., *92*, 9407-9414.

Fehler, M.C., Phillips, W.S., House, L.S., Jones, R.H., Aster, R. and Rowe, C.A. (2000), *A method for improving relative earthquake locations*, Bull. Seism. Soc. Am., *in press*.

Ferrazzini, V., Chouet, B., Fehler, M.C, and Aki, K. (1990), *Quantitative analysis of long period events recorded during hydrofracture experiments at Fenton Hill, New Mexico*, J. Geophys. Res., *95*, 21871-21884.

Fix, J.E., Adair, R.G., Fisher, T., Mahrer, K., Mulcahy, C., Myers, B., Swanson, J., and Woerpel, J.C. (1989), *Development of microseismic methods to determine hydraulic fracture dimensions*, Gas Res. Inst., Tech. Rep. No. 89-0116.

Franke, P. R., and Nunz, G.J. (1985), *Recent developments in the hot dry rock geothermal energy program*, Geothermal Resources Council Annual Meeting, Preprints, *1-4*.

Gaucher, E., Cornet, F.H. and Bernard, P. (1998). *Induced seismicity analysis for structure identification and stress field determination*, paper SPE 47324, Proc. SPE/ISRM, Trondhiem, Norway.

Hamilton-Smith, T., Nuttal, B.C., Gooding, P.J., Walker, D. and Drahovzal, J.A. (1990), *High volume oil discovery in Clinton County, Kentucky*, Kentucky Gol. Surv., Ser. 11, Inf. Circ. 33.

House, L. S., and Jensen, B. (1987), *Focal mechanisms of microearthquakes induced by hydraulic injection in crystalline rock*, EOS Trans., *68*, 1346.

House, L. S. (1987), *Locating microearthquakes induced by hydraulic fracturing in crystalline rock*, Geophys. Res. Lett., *14*, 919-921.

House, L.S., Flores, R. and Withers, R. (1996), *Microearthquakes induced by a hydraulic injection in sedimentary rock, east Texas*, SEG 66th Ann. Meeting, 110-113.

House, L.S. and Flores, R. (2000), *Seismological studies of a fluid injection in sedimentary rocks, east Texas*, submitted to Pure Appl. Geophys.

Jones, R.H. and Stewart, R.C. (1997). *A method for determining significant structures in a cloud of earthquakes*, J. Geophys. Res. *102*, 8245-8254.

Jones, R.H., Beauce, A., Jupe,A., Fabriol, H. and Dyer, B.C. (1995), *Imaging induced microseismicity during the 1993 injection tests at Soultz-sous-Forets, France*, Proc. World Geotherm. Cong., Florence, 2665-2669.

Jung, R., Rummel, F., Jupe, A., Bertozzi, A., Heinemann, B. and Wallroth, T. (1996). *Large scale hydraulic injections in the granitic basement in the European HDR programme at Soultz, France*, Proc. 3rd Int. HDR Forum, Santa Fe, 75-76.

Keck, R.G. and Withers, R.J. (1994), *A field demonstration of hydraulic fracturing for solid waste injection with real-time passive seismic monitoring*, paper SPE 28495, SPE Annual Technical Conference and Exhibition, New Orleans.

Kohl, T., Evans, K.F., Hopkirk, R.J., Jung, R. and Rybach, L. (1997). *Observation and simulation of non-Darcian flow transients in fractured rock*, Water Resour. Res., *33*, 407-418.

Lees, J.M. (1998), *Multiplet analysis at Coso geothermal*, Bull. Seism. Soc. Am., *88*, 1127-1143.

Li, Y.P., Cheng, C.H. and Toksoz, M.N. (1998), *Seismic monitoring of the growth of a hydraulic fracture zone at Fenton Hill, New Mexico*, Geophysics, *63*, 120-131.

Maxwell, S.C., Young, R.P., Bossu, R., Jupe, A. and Dangerfield, J. (1998), *Microseismic logging of the Ekofisk reservoir*, paper SPE 47276, Proc. SPE/ISRM, Trondhiem, Norway.

Moriya, H., Nagano, K. and Niitsuma, H. (1994), *Precise source location of AE doublets by spectral matrix analysis of triaxial hodogram*, Geophysics, *59*, 36-45.

Pearson, C. (1981), *The relationship between microseismicity and high pore pressures during hydraulic stimulation experiments in low permeability granitic rocks*, J. Geophys. Res., *86*, 7855-7864.

Phillips, W.S., House, L.S. and Fehler, M.C. (1997), *Detailed joint structure in a*

geothermal reservoir from studies of induced microearthquake clusters, J. Geophys. Res., *102*, 11745-11763.

Phillips, W.S., Fairbanks, T.D., Rutledge, J.T. and Anderson, D.W. (1998), *Induced microearthquake patterns and oil-producing fracture systems in the Austin chalk*, Tectonophysics, *289*, 153-169.

Phillips, W.S. (2000), *Precise microearthquake locations and fluid flow in the geothermal reservoir at Soultz-sous-Forêts, France*, Bull. Seism. Soc. Am., *90*, 212-228.

Rieven, S.A. (1999), *Analysis and interpretation of clustered microseismicity at geothermal and petroleum reservoirs*, Ph.D. Thesis, MIT, Cambridge, 410 pp.

Roff, A., Phillips, W.S. and Brown, D.W. (1996), *Joint structures determined by clustering microearthquakes using waveform amplitude ratios*, Int. J. Rock Mech. Geomech. Abs., *33*, 627-639.

Rubin, A.M., Gillard, D. and Got, J.-L. (1999), *Streaks of microearthquakes along creeping faults*, Nature, *400*, 635-641.

Rutledge, J.T., Phillips, W.S., House, L.S. and Zinno, R.J. (1998a), *Microseismic mapping of a Cotton Valley hydraulic fracture using decimated downhole arrays*, Proc. 68th Ann. Mtg., SEG, 338-341.

Rutledge, J.T., Phillips, W.S. and Schuessler, B.K. (1998b), *Reservoir characterization using oil-production-induced microseismicity, Clinton County, Kentucky*, Tectonophysics. *289*, 129-152.

Sarda, J.-P., Perreau, P.J. and Deflandre, J.-P., *Acoustic emission interpretation for estimating hydraulic fracture extent*, paper SPE 17723, SPE Gas Technology Symposium, Dallas.

Shearer, P.M. (1997), *Improving local earthquake locations using the L1 norm and waveform cross correlation: Application to the Whittier Narrows, California, aftershock sequence*, J. Geophys. Res. *102*, 8269-8284.

Sykes, L.R. (1970), *Earthquake swarms and sea-floor spreading*, J. Geophys. Res., *75*,

6598-6611.

Tezuka, K. and Niitsuma, H. (1997), *Integrated interpretation of microseismic clusters and fracture system in a Hot Dry Rock artificial reservoir*, Proc. 67th Ann. Mtg., SEG, 657-660.

VanDecar, J.C. and Crosson, R.S. (1990), *Determination of teleseismic relative phase arrival times using multi-channel cross-correlation and least squares*, Bull. Seism. Soc. Am. *80*, 150-169.

Vinegar, H. J., Wills, P.B., DeMartini, D.C., Shylapobersky, J., Deeg, W.F., Adair, R.G., Woerpel, J.C., Fix, J.E. and Sorrells, G.G. (1991), *Active and passive seismic imaging of a hydraulic fracture in diatomite*, paper SPE 22756, SPE Annual Technical Conference and Exhibition, Dallas.

Walker, R.N. (1997), *Cotton Valley hydraulic fracture imaging project*, SPE paper 38577, SPE Annual Technical Conference and Exhibition, San Antonio.

Warpinski, N.R. and Teufel, L.W. (1987), *Influence of geologic discontinuities on hydraulic fracture propagation*, J. Pet. Tech., *39*, 209.

Warpinski, N.R., Wright, T.B., Uhl, J.E., Engler, B.P, Drozda, P.M., Peterson and Branagan, P.T. (1996), *Microseismic monitoring of the B-sand hydraulic fracture experiment at the DOE/GRI Multi-Site project*, paper SPE 36450, SPE Annual Technical Conference and Exhibition, Denver.

Withers, R.J. and Rieven, S.A. (1996), *Fracture development during cuttings injection determined by passive seismic monitoring*, SEG 66th Ann. Meeting, 106-109.

Zhu, X., Gibson, J., Ravindran, N., Zinno, R., Sixta, D. (1996), *Seismic imaging of hydraulic fractures in Carthage tight sands: A pilot study*, The Leading Edge, *15*, 218-224.

Figure Captions

Figure 1. Number of recorded events versus injection volume from a sample of crystalline and sedimentary reservoir experiments. Crystalline rock experiments are represented by filled circles and include many Fenton Hill injections. Sedimentary experiments are represented by open circles. The Colorado basin experiment produced no observable events, as indicated by an arrow. Results from a Cotton Valley injection coincides with a Fenton Hill experiment as indicated by a second arrow.

Figure 2. Vertical component seismograms generated by six events during the MHF injection at Fenton Hill. The top three events occur in the cluster shown in Figure 8. The bottom three occur in a separate cluster, as described in Phillips et al., 1997.

Figure 3. Cross section and map views of events located in the Austin chalk at the Matcek site, Giddings field, Texas. Monitor and injection wells are shown and depths indicated by solid circles in the cross section. Event locations are indicated by open circles. Error ellipses for representative events are included.

Figure 4. Map and cross-section views of events located in the lower Frio during the waste injection experiment. Monitor and injection wells are indicated by open circles in the map view. Arrows show cross-section view directions. In cross-section views, wells are indicated by light gray lines; thick lines represent locations of geophone strings. The gap in the injection well represents the injection interval. Only events from the linear cluster located southwest of the injection well are included in the cross-section views.

Figure 5. Map and cross section views of a relocated cluster of Cotton Valley events. Colors represent event groups based on waveform type. Map view arrows give along and across trend cross-section view directions.

Figure 6. Spatio-temporal behavior of the Cotton Valley cluster. Events are represented by open circles whose diameters are proportional to peak log trace amplitude. Colors represent event groups based on waveform type as in Figure 5. The slurry (injection) rate is included on the left (peak rate 105 l/s). Activity associated with the third injection pulse is scaled up in the inset plot. Numbers represent sub-clusters of events discussed in the text.

Figure 7. Map (top) and cross-section (bottom) views of seismicity recorded at the Tallent site, Clinton County, Kentucky. In the map view, the current producing well is represented by a star, monitor wells by triangles and remaining production wells by open circles. Event locations are represented by dots with colors indicating one of three fractures. An arrow indicates the cross-section view direction. In the cross-section view, wells existing prior to geophone deployment are indicated by solid lines, wells drilled following deployment by dotted lines. Old production intervals are represented by squares, the current producing interval by a star and geophone positions by triangles. Possible aseismic fractures are indicated by dashed lines. Only seismicity that occurred east of –20 m is included in the cross-section plot.

Figure 8. Map and cross-section views of a relocated Fenton Hill cluster. Arrows indicate cross-section view angles (map view) and edges discussed in the text (broadside view).

Figure 9. Cross-section views of two relocated Soultz clusters. The shallow cluster is shown on the left, the deep cluster on the right. Top views are along the trends of the fracture intersection axes. Bottom views are broadside to plane 1 and plane 3. Projected focal mechanisms are indicated in the along axis views. A dashed line divides shallow cluster planes based on P-polarity patterns. Red and blue represent deep cluster events grouped by waveform shape. In the broadside views, colors represent the order in which the earliest half of the events occurred. Various linear features discussed in the text are indicated by the annotated arrows.

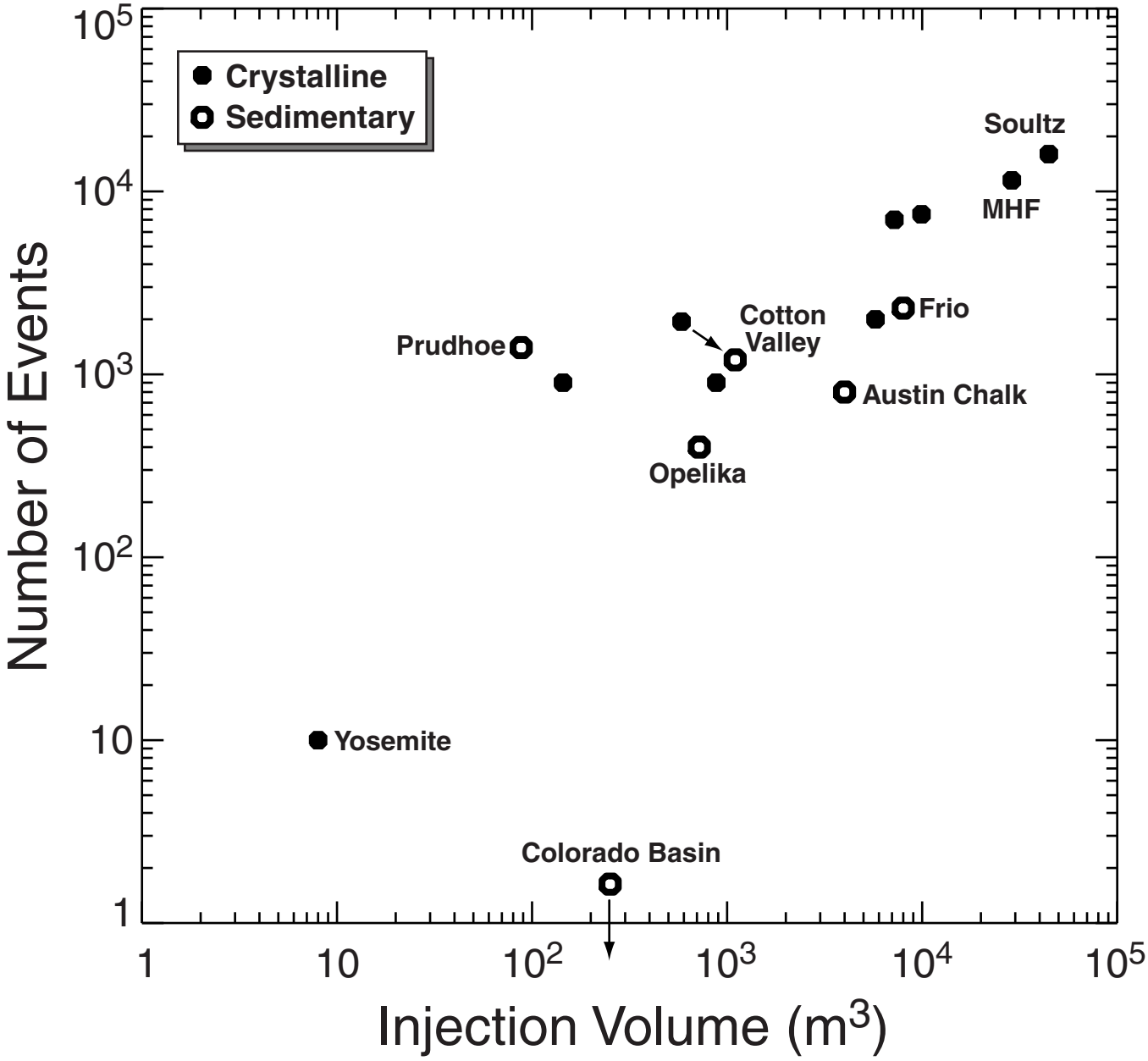
Crystalline
Sedimentary
Soultz
MHF
Frio
Cotton
Valley
Prudhoe
Austin Chalk
Opelika
Yosemite
Colorado Basin
Number of Events
Injection Volume (m3)
10^5
10^4
10^3
10^2
10
1
1
10
10^2
10^3
10^4
10^5

Figure 1

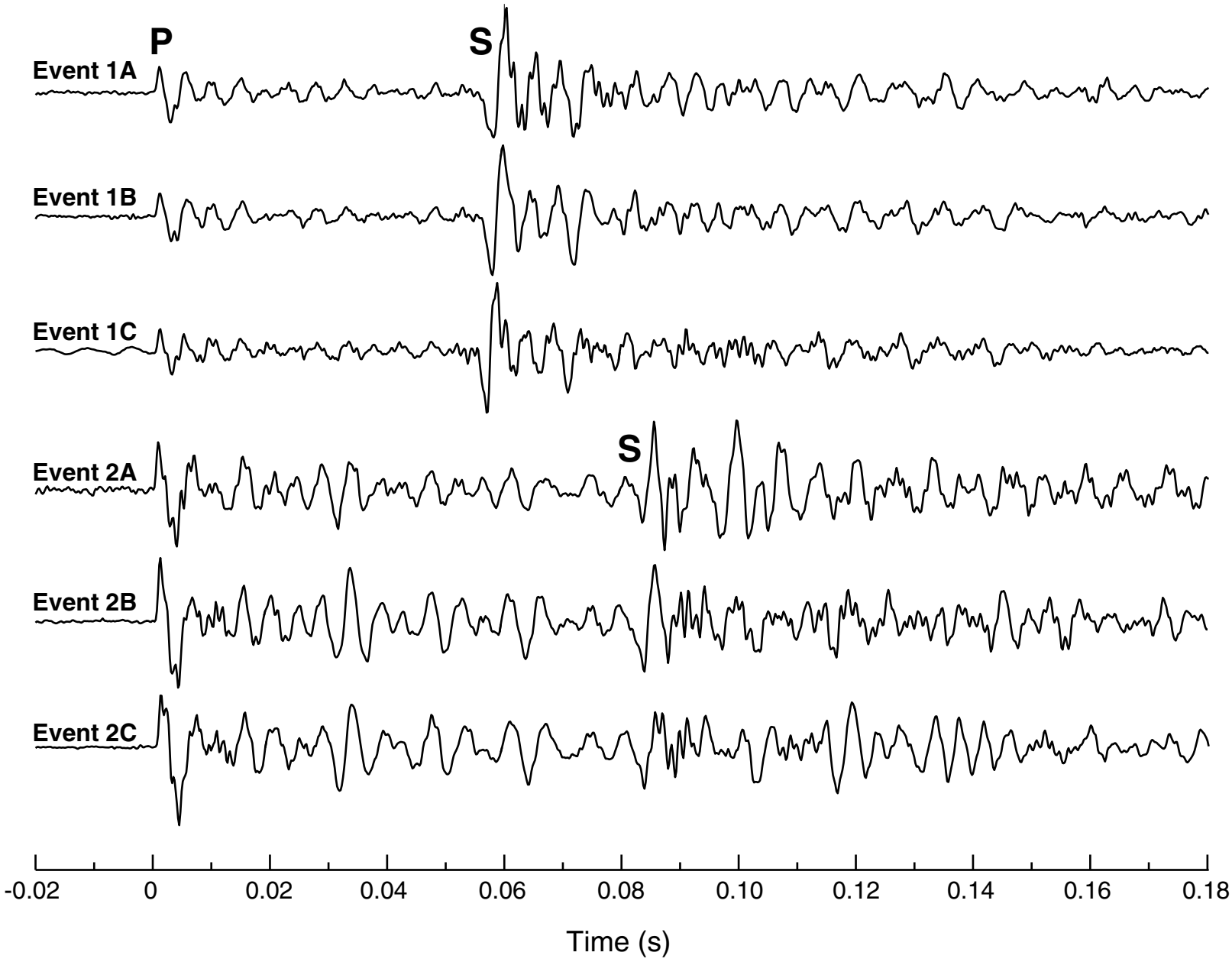
P
S
Event 1A
Event 1B
Event 1C
S
Event 2A
Event 2B
Event 2C
-0.02
0
0.02
0.04
0.06
0.08
0.10
0.12
0.14
0.16
0.18
Time (s)

Figure 2

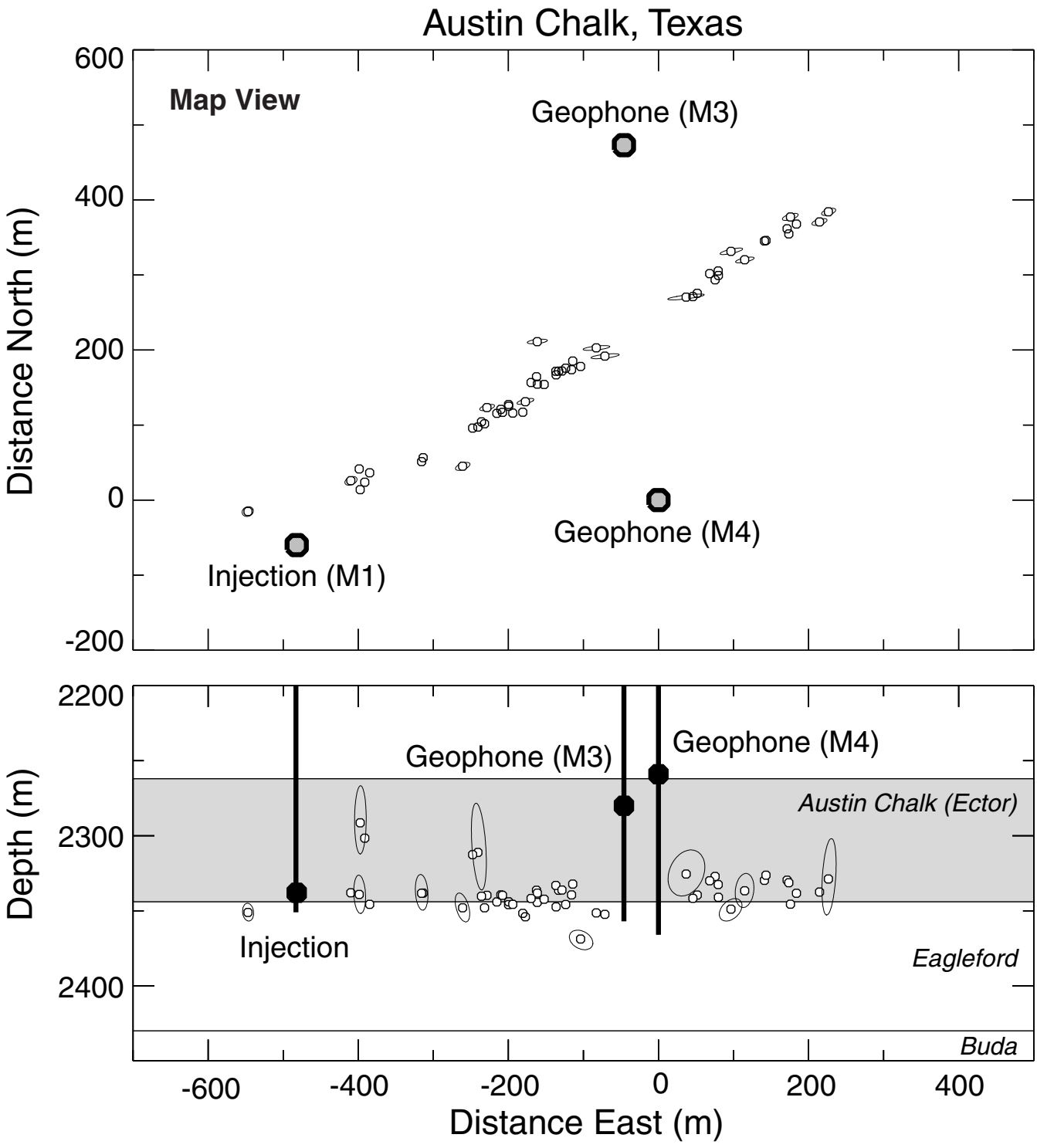
Austin Chalk, Texas
Map View
Geophone (M3)
Geophone (M4)
Injection (M1)
Distance North (m)
600
400
200
0
-200
Geophone (M3)
Geophone (M4)
Austin Chalk (Ector)
Injection
Eagleford
Buda
Depth (m)
2200
2300
2400
-600
-400
-200
0
200
400
Distance East (m)

Figure 3

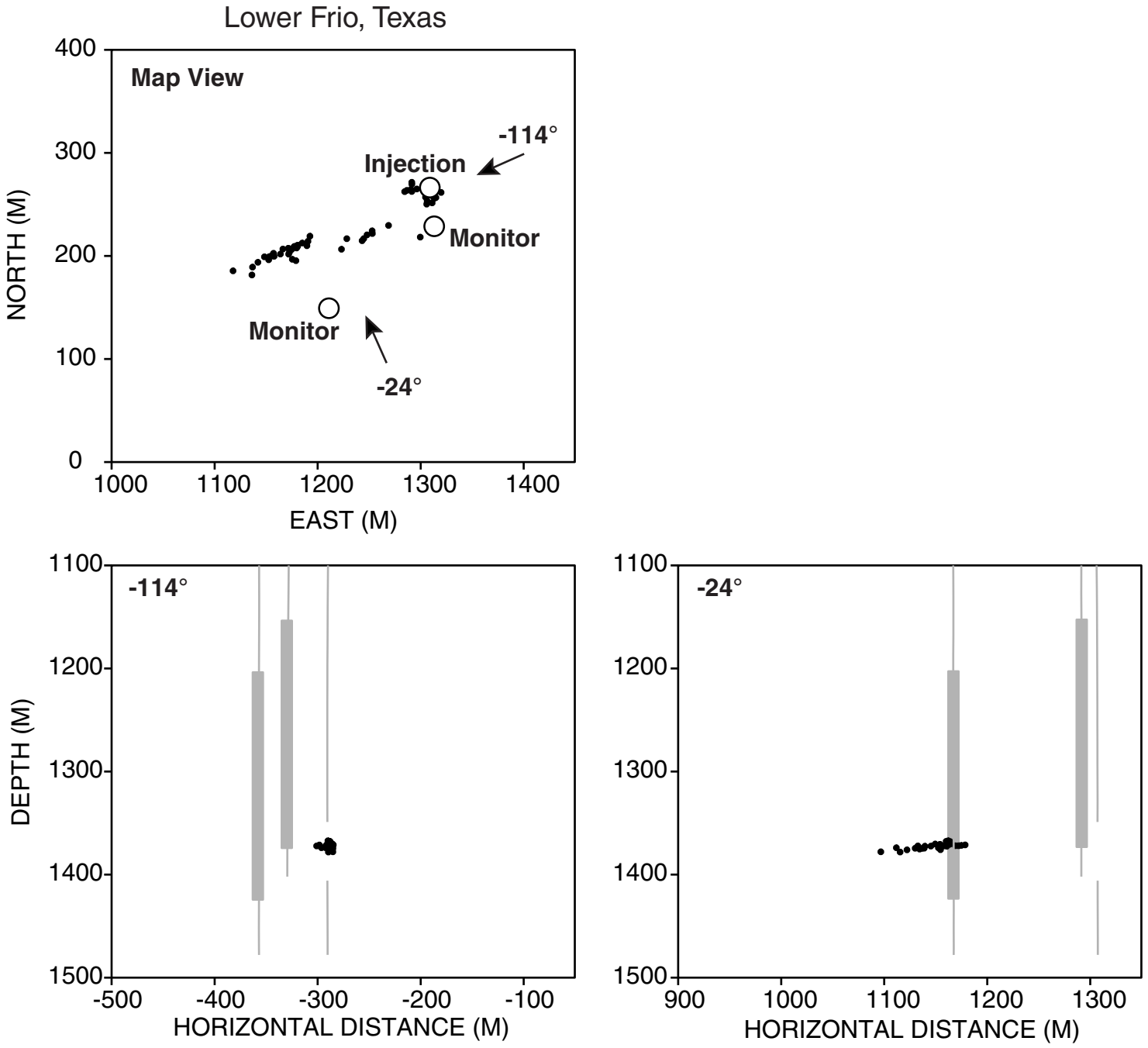
Lower Frio, Texas
Map View
-114°
Injection
Monitor
Monitor
-24°
NORTH (M)
EAST (M)
400
300
200
100
0
1000
1100
1200
1300
1400
-114°
-24°
DEPTH (M)
HORIZONTAL DISTANCE (M)
HORIZONTAL DISTANCE (M)
1100
1200
1300
1400
1500
-500
-400
-300
-200
-100
900
1000
1100
1200
1300

Figure 4

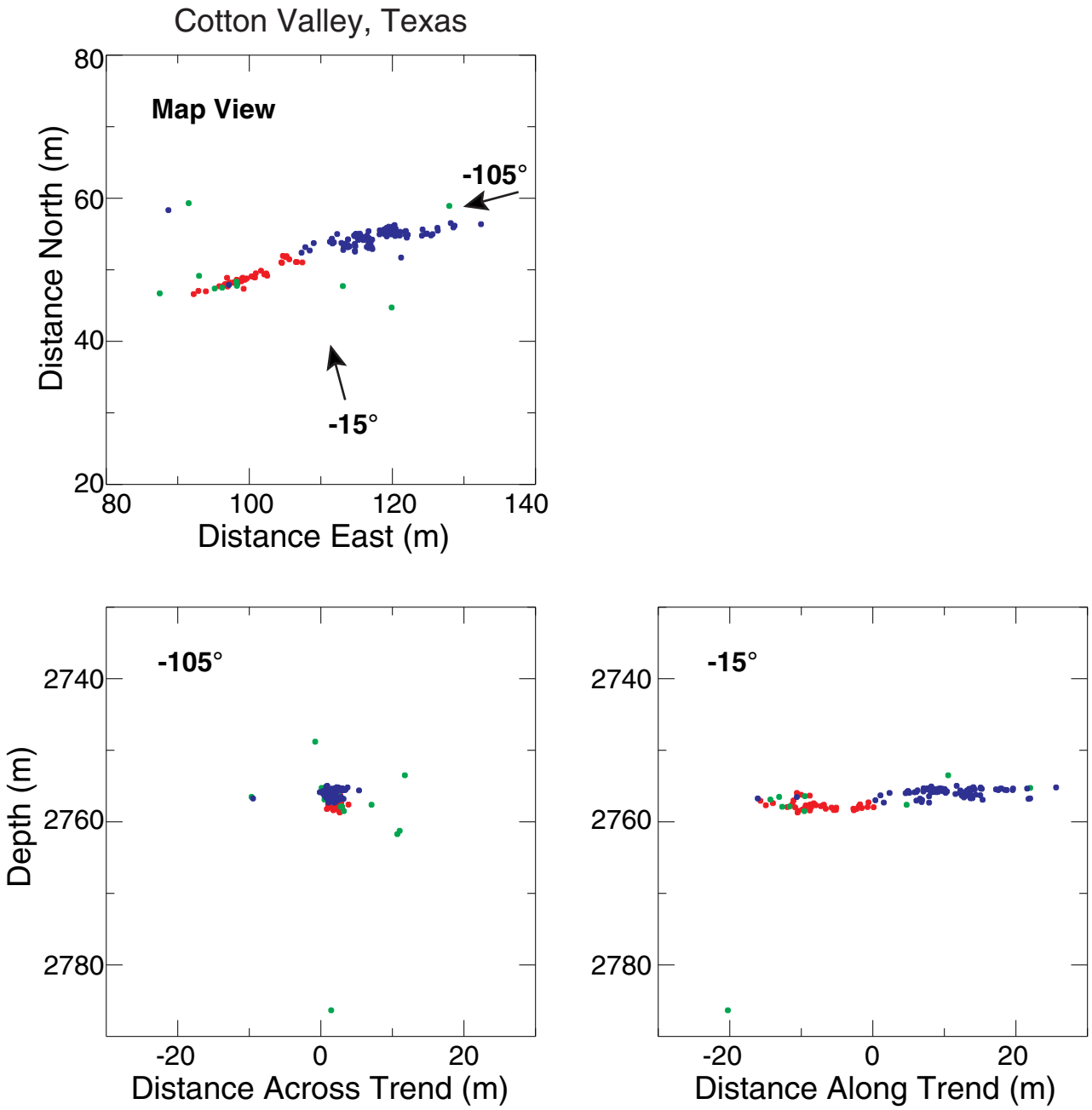
Cotton Valley, Texas
Map View
-105°
-15°
Distance North (m)
Distance East (m)
80
60
40
20
80
100
120
140
-105°
-15°
Depth (m)
2740
2760
2780
-20
0
20
Distance Across Trend (m)
Distance Along Trend (m)

Figure 5

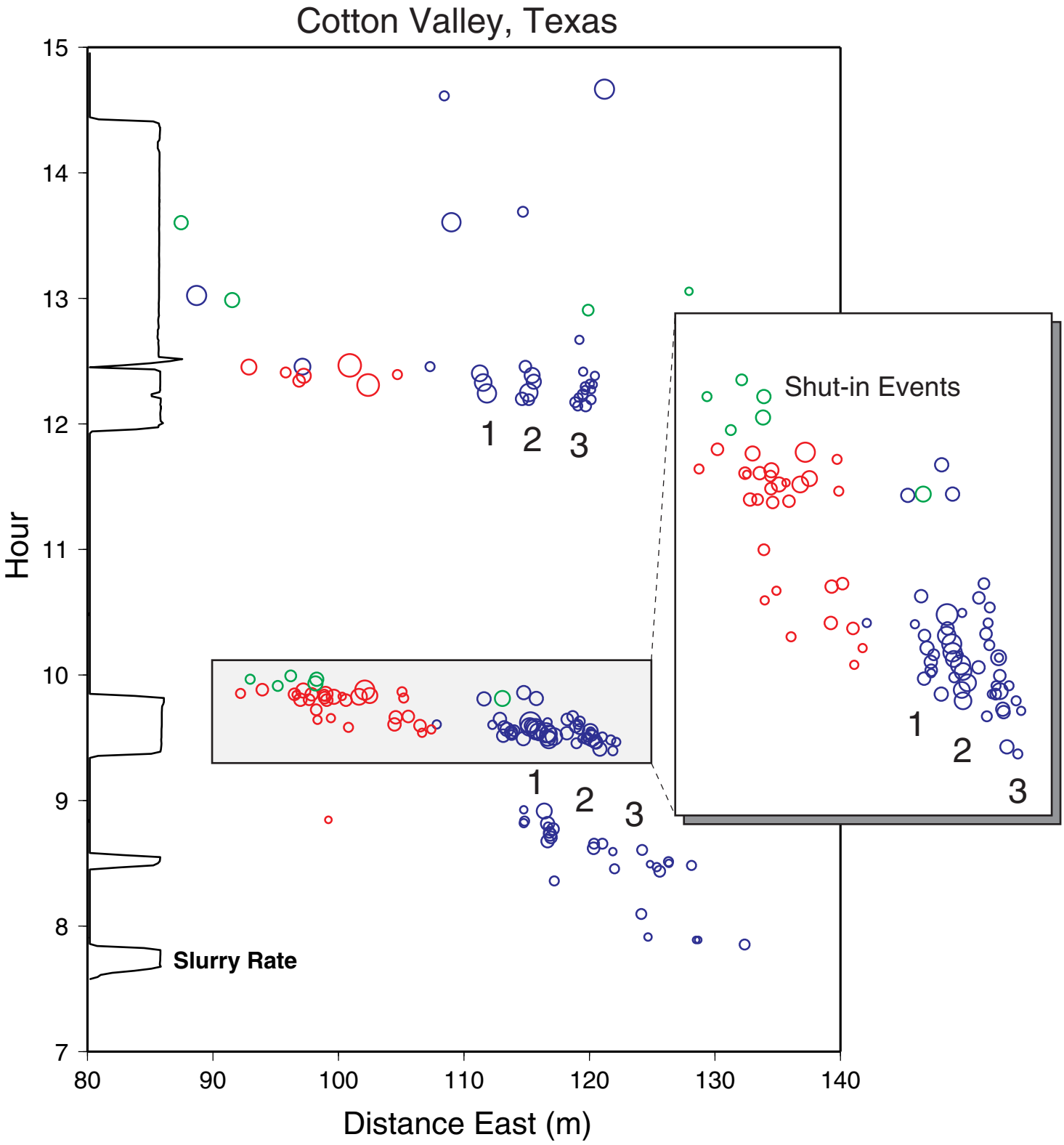
Cotton Valley, Texas
Hour
Distance East (m)
Slurry Rate
Shut-in Events
1
2
3
15
14
13
12
11
10
9
8
7
80
90
100
110
120
130
140

Figure 6

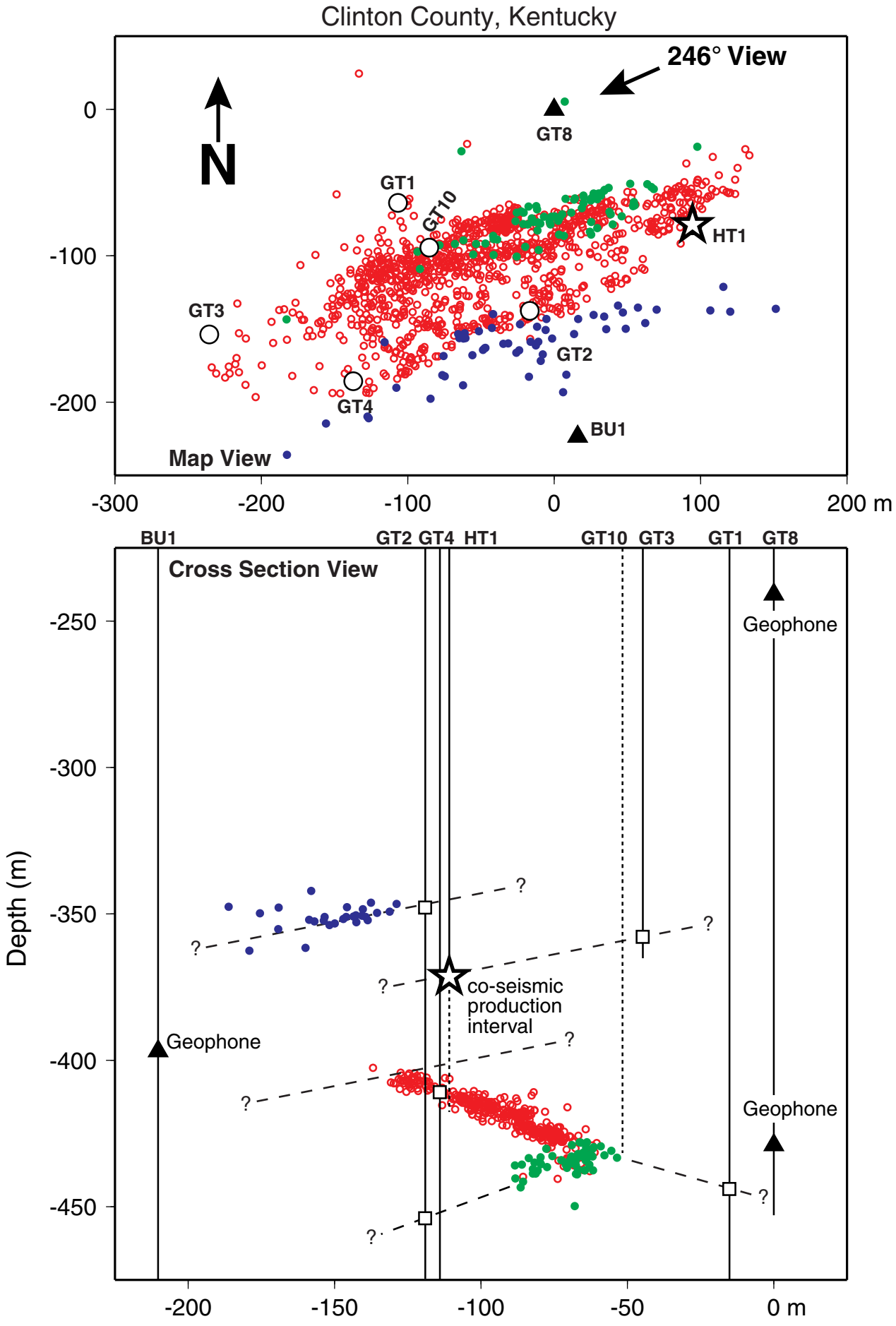
Clinton County, Kentucky
246° View
N
GT8
GT1
GT10
HT1
GT3
GT2
GT4
BU1
Map View
0
-100
-200
-300
-200
-100
0
100
200 m
BU1
GT2 GT4 HT1
GT10 GT3
GT1 GT8
Cross Section View
Depth (m)
-250
-300
-350
-400
-450
Geophone
co-seismic
production
interval
Geophone
Geophone
-200
-150
-100
-50
0 m

Figure 7

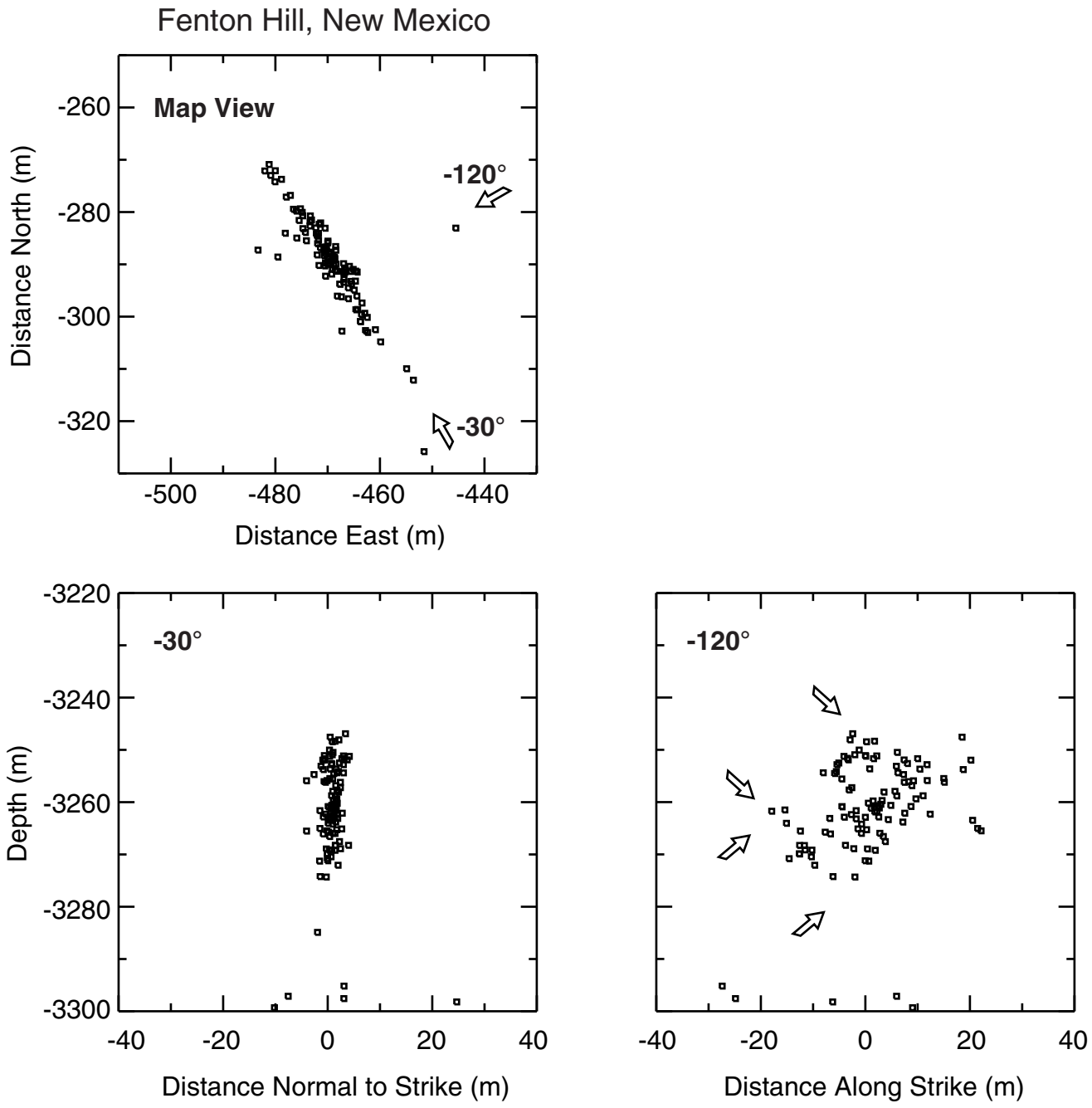
Fenton Hill, New Mexico
Map View
-120°
-30°
Distance North (m)
-260
-280
-300
-320
-500
-480
-460
-440
Distance East (m)
-30°
Depth (m)
-3220
-3240
-3260
-3280
-3300
-40
-20
0
20
40
Distance Normal to Strike (m)
-120°
-40
-20
0
20
40
Distance Along Strike (m)

Figure 8

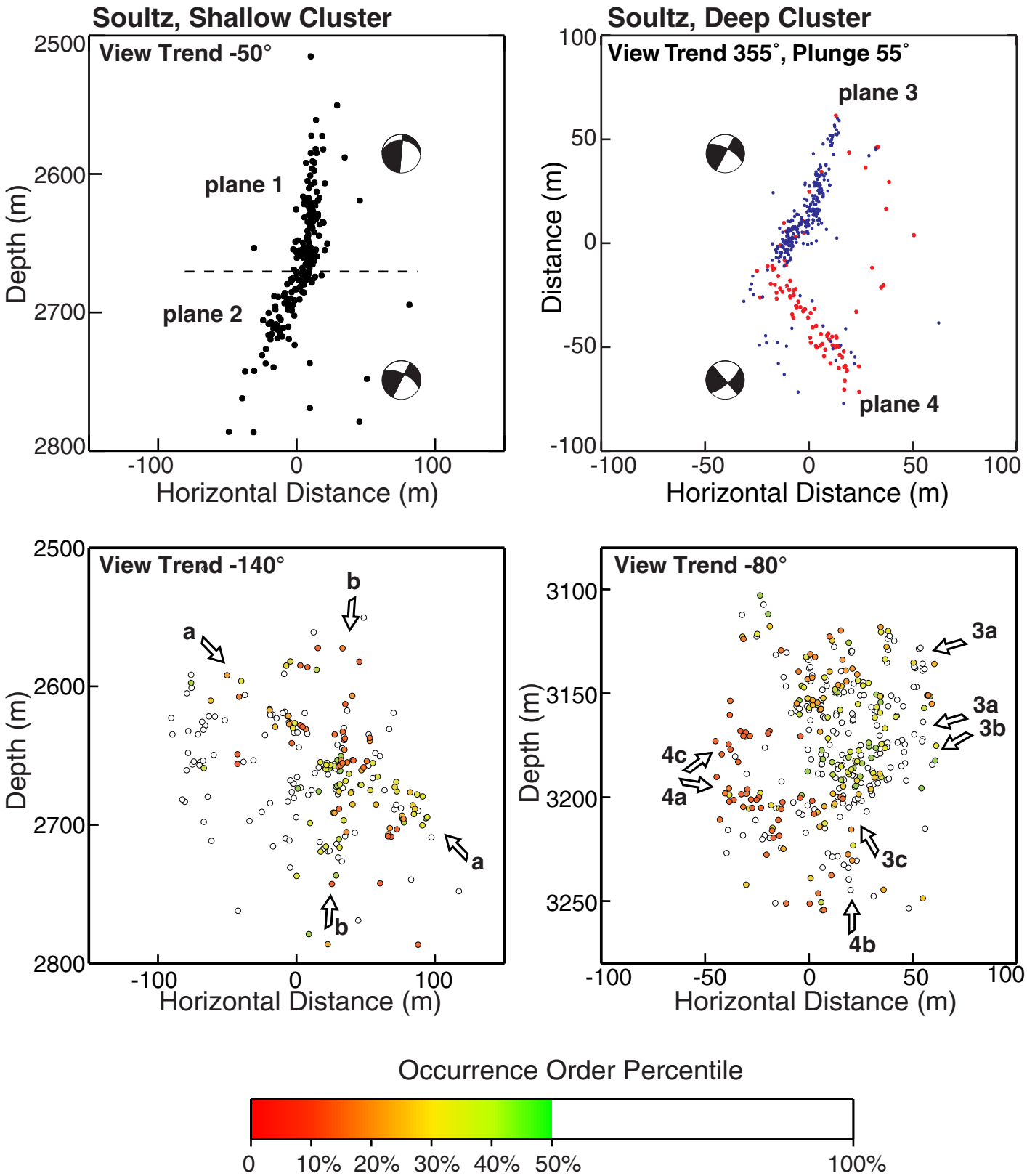
Soultz, Shallow Cluster
View Trend -50°
plane 1
plane 2
Depth (m)
Horizontal Distance (m)
Soultz, Deep Cluster
View Trend 355°, Plunge 55°
plane 3
plane 4
Distance (m)
Horizontal Distance (m)
View Trend -140°
a
b
Depth (m)
Horizontal Distance (m)
View Trend -80°
3a
3a
3b
4c
4a
3c
4b
Depth (m)
Horizontal Distance (m)
Occurrence Order Percentile
0
10%
20%
30%
40%
50%
100%

Figure 9